

Supplemental Material A: Observations of and calculations for each snowpit

Table 1A. Description of snowpits dug during the UBWOS 2014 campaign.

Pit	Date Time	Meteorology	Snow depth (cm)
1	Jan. 15 10:00-13:00	Clear, calm winds, Air temperature <sup>1</sup> : -10°C, -3°C	18
2	Jan. 17 9:00-14:00	Clear, calm winds, Air temperature <sup>1</sup> : -10°C, -3°C	9
3	Jan. 20 10:00-13:00	Clear, calm winds, Air temperature <sup>1</sup> : -9°C, -4°C	14
4	Jan. 22 10:00-13:00	Clear, calm winds, Air temperature <sup>1</sup> : -15°C, -1°C	18
5	Jan. 24 10:00-12:00	Clear, calm winds, Air temperature <sup>1</sup> : -14°C, -9°C	11
6	Jan. 26 10:00-13:00	Clear, calm winds, Air temperature <sup>1</sup> : -6°C, -2°C	18
7	Jan. 29 10:30-12:30	Cloudy, calm winds, Air temperature <sup>1</sup> : -10°C, -5°C	20
8	Jan. 30 10:00-11:30	Cloudy, calm winds, light snow Air temperature <sup>1</sup> : -2°C, -1°C	15
9	Jan. 31 13:00-14:30	Partly cloudy, calm winds Air temperature <sup>1</sup> : -2°C, -1°C	14
10	Feb. 4 10:00-12:30	Cloudy, calm winds Air temperature <sup>1</sup> : -8°C, -2°C	24
11	Feb. 6 10:00-12:00	Cloudy, calm winds, Air temperature <sup>1</sup> : -13°C, -7°C	21
12	Feb. 11 9:00-10:30	Cloudy, calm winds, Air temperature <sup>1</sup> : -2°C, 2°C	20

<sup>1</sup>Temperature was measured before and after each snowpit was dug.

Table 2A. Vertical profiles of snow temperature (K). Snow temperature was not measured for snowpits 1, 2, and 3.

Snowpit	Temperature (K) at various depths
1	Temperature not measured
2	Temperature not measured
3	Temperature not measured
4	0-18 cm: 267
5	0-11 cm: 267
6	0-7 cm: 273 7-18 cm: 267
7	0-7 cm: 271 7-17 cm: 268 17-20 cm: 268
8	0-4 cm: 273 4-12 cm: 271 12-15: 270
9	0-14 cm: 272
10	0-3 cm: 265 3-10 cm: 266 10-21 cm: 267 21-24 cm: 269
11	0-3 cm: 258 3-10 cm: 260 10-17 cm: 261 17-21 cm: 263
12	0-3 cm: 271 3-20: 272

Table 3A. Snow photic zone depth, modeled  $F_{Nr}$  using only E8, and daily-averaged  $F_{Nr}$  calculated using TRANSITS for all snowpits.

Pit	Photic zone depth (cm)	$F_{Nr}$ (E8, SZA=65°) (molec cm <sup>-2</sup> s <sup>-1</sup> )	Daily-averaged $F_{Nr}$ (TRANSITS) (molec cm <sup>-2</sup> s <sup>-1</sup> )	Daily-maximum $F_{Nr}$ (TRANSITS) (molec cm <sup>-2</sup> s <sup>-1</sup> )
1	8.5	1.2x10 <sup>9</sup>	5.4x10 <sup>8</sup>	2.6x10 <sup>9</sup>
2	5.5	7.7x10 <sup>8</sup>	5.6x10 <sup>8</sup>	2.6x10 <sup>9</sup>
3	5.5	7.3x10 <sup>8</sup>	6.0x10 <sup>8</sup>	2.9x10 <sup>9</sup>
4	5.0	5.6x10 <sup>8</sup>	6.3x10 <sup>8</sup>	3.0x10 <sup>9</sup>
5	6.5	8.0x10 <sup>8</sup>	6.5x10 <sup>8</sup>	3.0x10 <sup>9</sup>
6	6.0	5.9x10 <sup>8</sup>	6.8x10 <sup>8</sup>	3.1x10 <sup>9</sup>
7	5.5	5.6x10 <sup>8</sup>	7.1x10 <sup>8</sup>	3.1x10 <sup>9</sup>
8	7.0	1.0x10 <sup>9</sup>	7.2x10 <sup>8</sup>	3.1x10 <sup>9</sup>
9	7.0	1.9x10 <sup>8</sup>	5.6x10 <sup>7</sup>	2.4x10 <sup>8</sup>
10	7.0	3.2x10 <sup>8</sup>	1.2x10 <sup>8</sup>	4.7x10 <sup>8</sup>
11	6.0	2.7x10 <sup>8</sup>	1.5x10 <sup>8</sup>	5.8x10 <sup>8</sup>
12	5.0	5.5x10 <sup>7</sup>	2.1x10 <sup>8</sup>	7.9x10 <sup>8</sup>

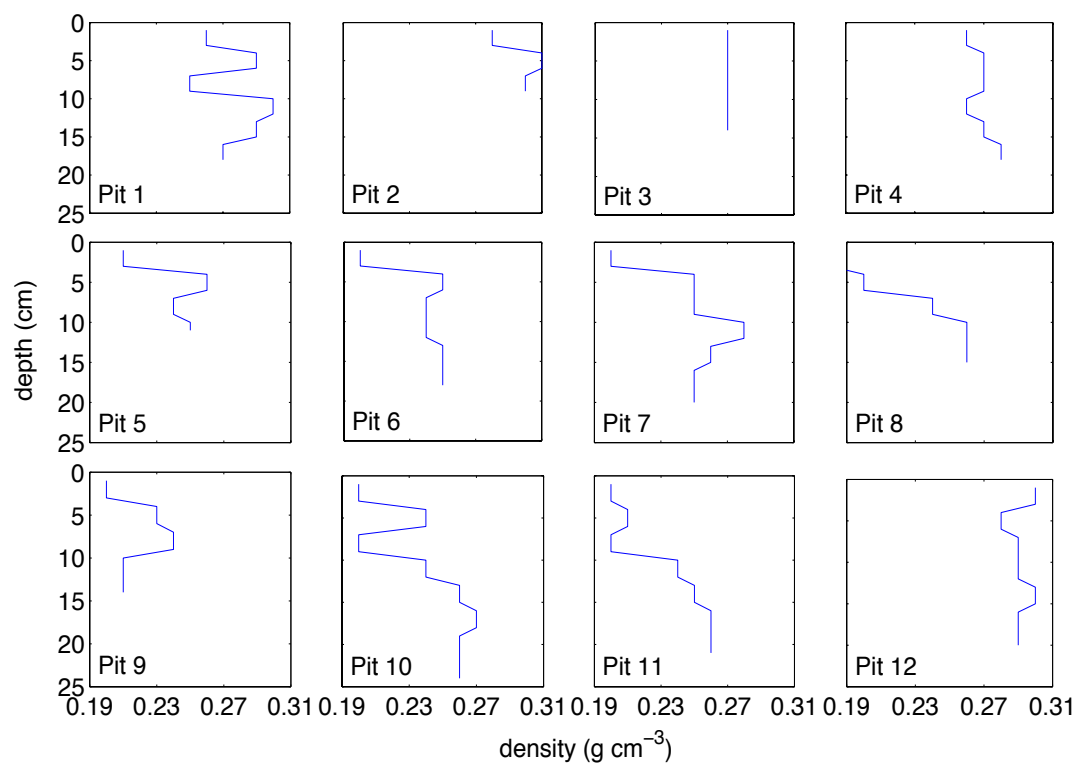


Figure 1A. Vertical profiles of snow density.

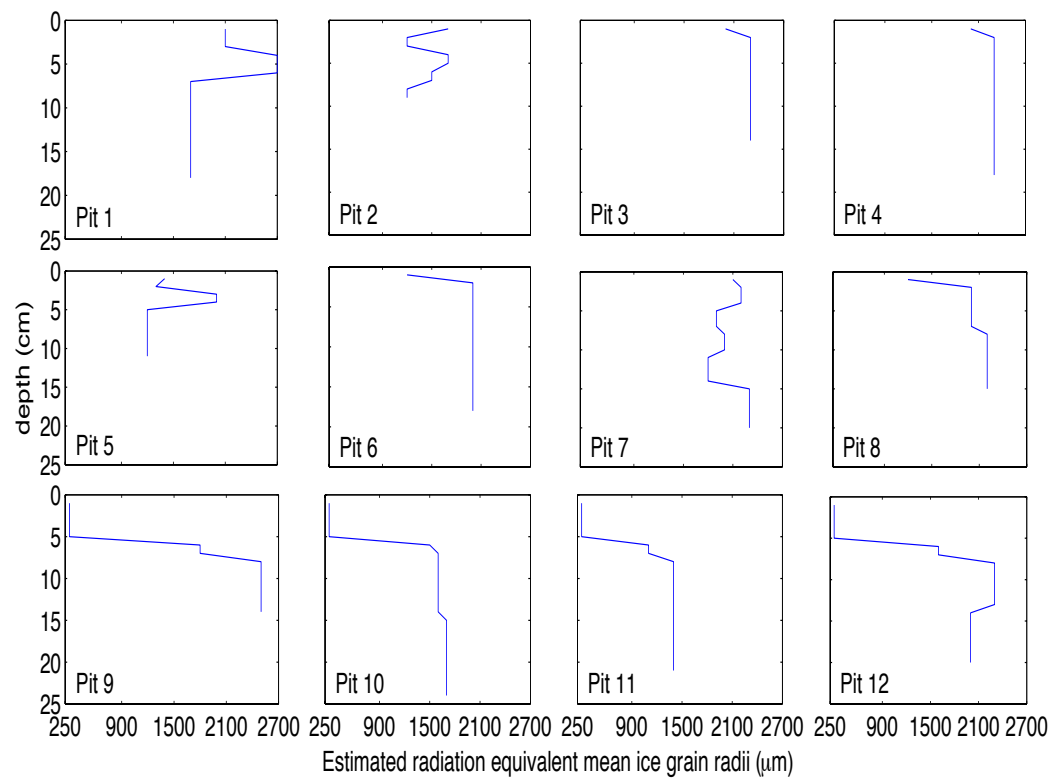


Figure 2A. Vertical profiles of visually-estimated radiation equivalent mean ice grain radii ( $\mu\text{m}$ ).

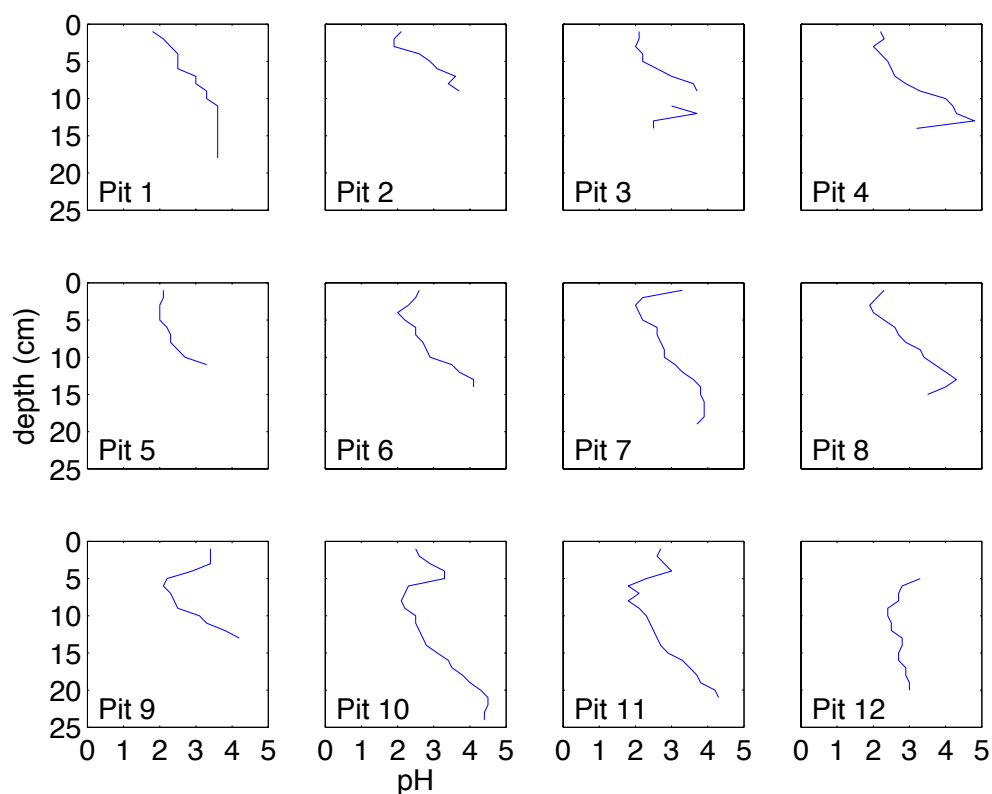


Figure 3A. Vertical profiles of pH in snow calculated using ion balance ( $[H^+] = [Cl^-] + [NO_3^-] + [SO_4^{2-}] - [Na^+] - [NH_4^+] - [K^+] - [Mg^{2+}] - [Ca^{2+}]$ ), where  $pH = -\log_{10}[H^+]$  and  $H^+$  is expressed in M.

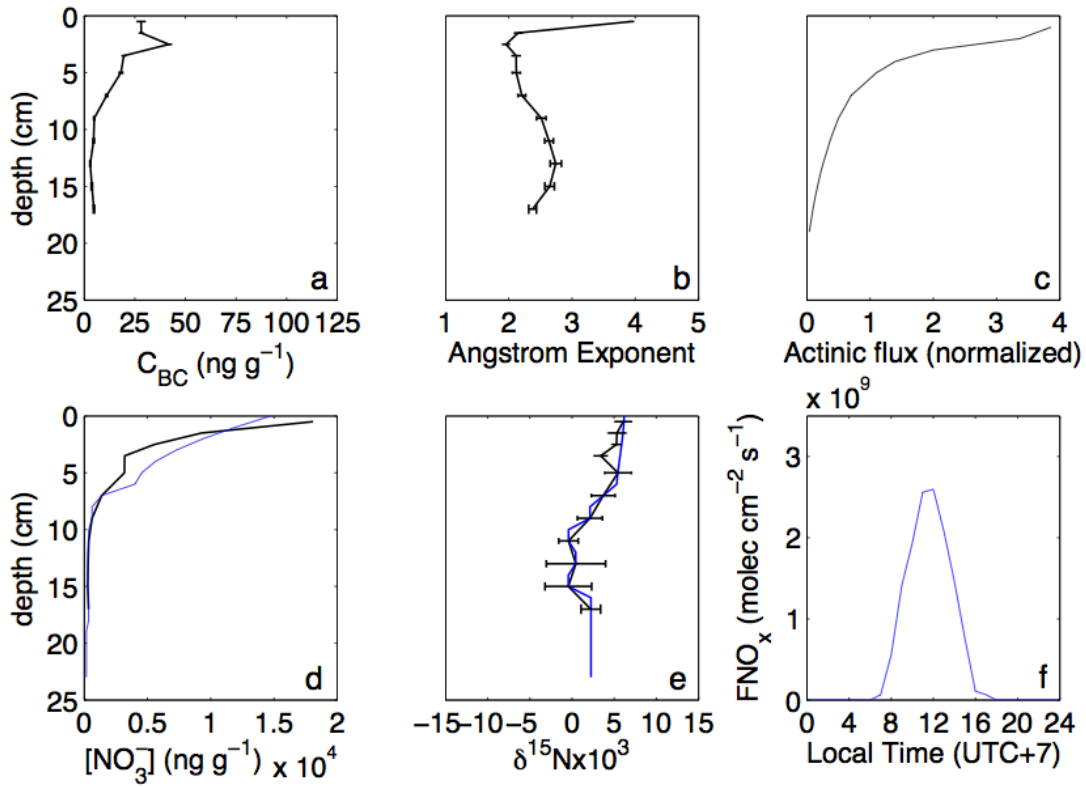


Figure 4A. Measured and modeled snow optical and chemical properties on January 15, 2014. Vertical profiles of (a) Measured black carbon concentrations ( $C_{BC}$ , ng g<sup>-1</sup>), (b) Measured Ångström exponent for  $\lambda=450-600$  nm (unitless), (c) UV actinic flux normalized to surface downwelling irradiance, (d) Measured (black) and modeled (blue) nitrate concentrations (ng g<sup>-1</sup>), (e) Measured (black) and modeled (blue)  $\delta^{15}N(NO_3^-)$  when  $\Phi=4.6 \times 10^{-3}$  (‰), (f) Diurnal profiles of modeled snow-sourced  $F_{Nr}$  (molec cm<sup>-2</sup> s<sup>-1</sup>) from TRANSITS.

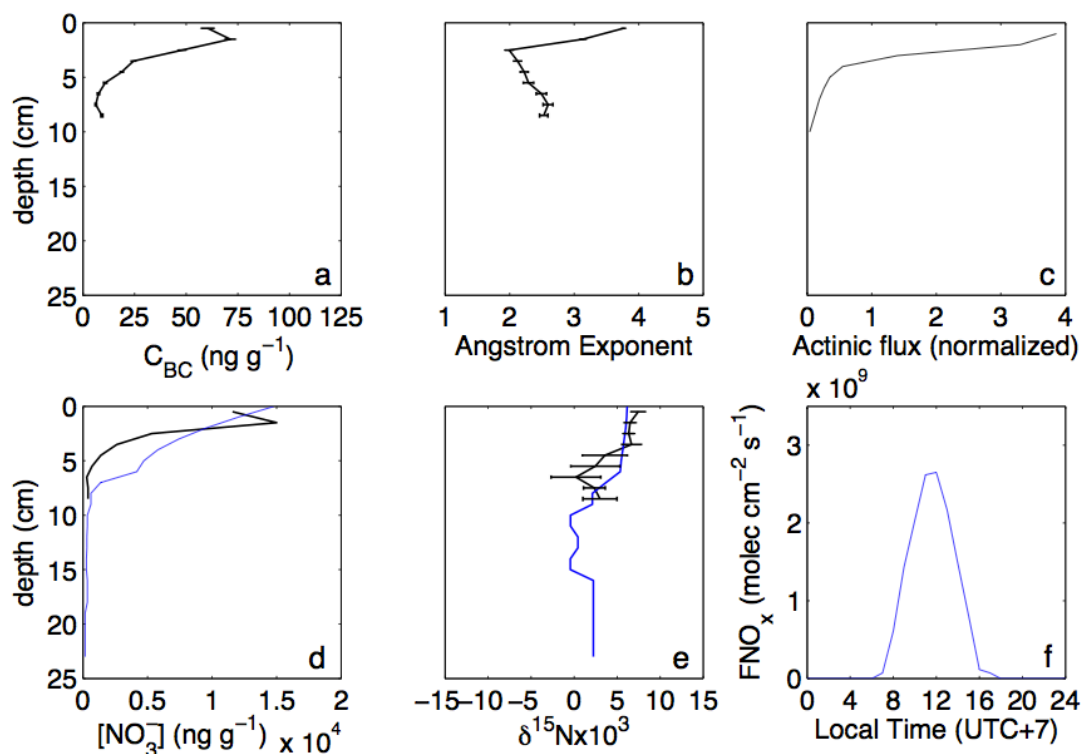


Figure 5A. Measured and modeled snow optical and chemical properties on January 17, 2014. Vertical profiles of (a) Measured black carbon concentrations ( $C_{BC}$ , ng g<sup>-1</sup>), (b) Measured Ångström exponent for  $\lambda=450-600$  nm (unitless), (c) UV actinic flux normalized to surface downwelling irradiance, (d) Measured (black) and modeled (blue) nitrate concentrations (ng g<sup>-1</sup>), (e) Measured (black) and modeled (blue)  $\delta^{15}N(NO_3^-)$  when  $\Phi=4.6 \times 10^{-3}$  (‰), (f) Diurnal profiles of modeled snow-sourced  $F_{Nr}$  (molec cm<sup>-2</sup> s<sup>-1</sup>) from TRANSITS.



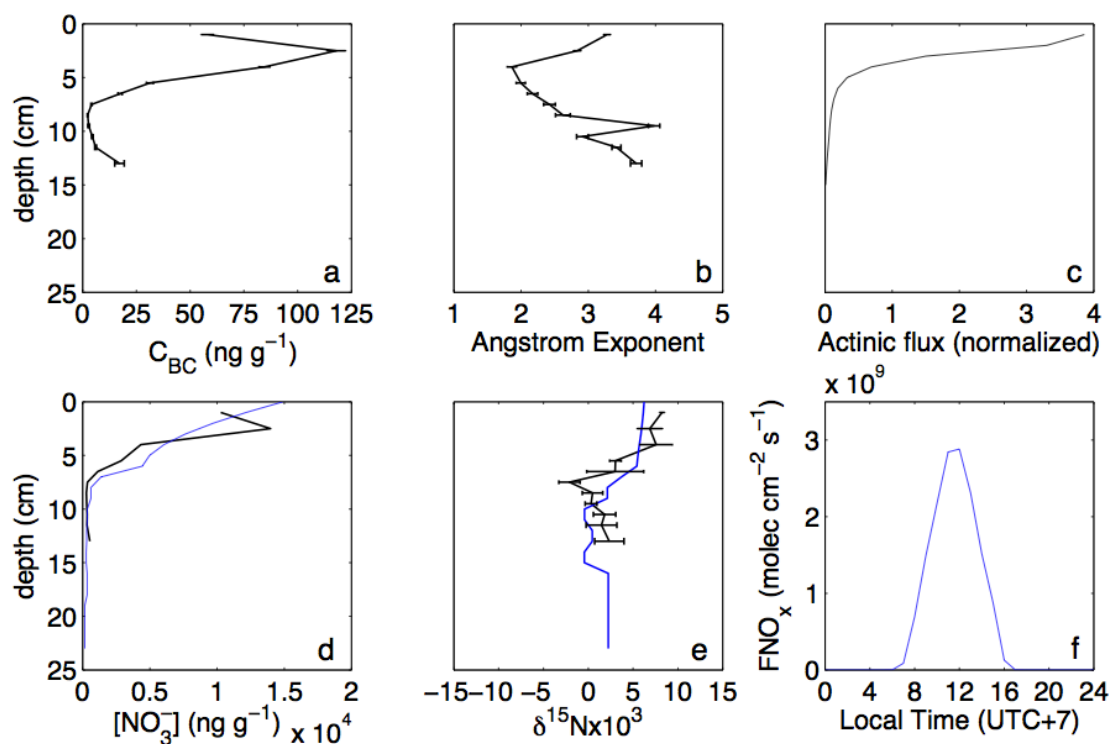


Figure 6A. Measured and modeled snow optical and chemical properties on January 20, 2014. Vertical profiles of (a) Measured black carbon concentrations ( $C_{BC}$ , ng g<sup>-1</sup>), (b) Measured Ångström exponent for  $\lambda=450-600$  nm (unitless), (c) UV actinic flux normalized to surface downwelling irradiance, (d) Measured (black) and modeled (blue) nitrate concentrations (ng g<sup>-1</sup>), (e) Measured (black) and modeled (blue)  $\delta^{15}N(NO_3^-)$  when  $\Phi=4.6 \times 10^{-3}$  (‰), (f) Diurnal profiles of modeled snow-sourced  $F_{NO_x}$  (molec cm<sup>-2</sup> s<sup>-1</sup>) from TRANSITS.

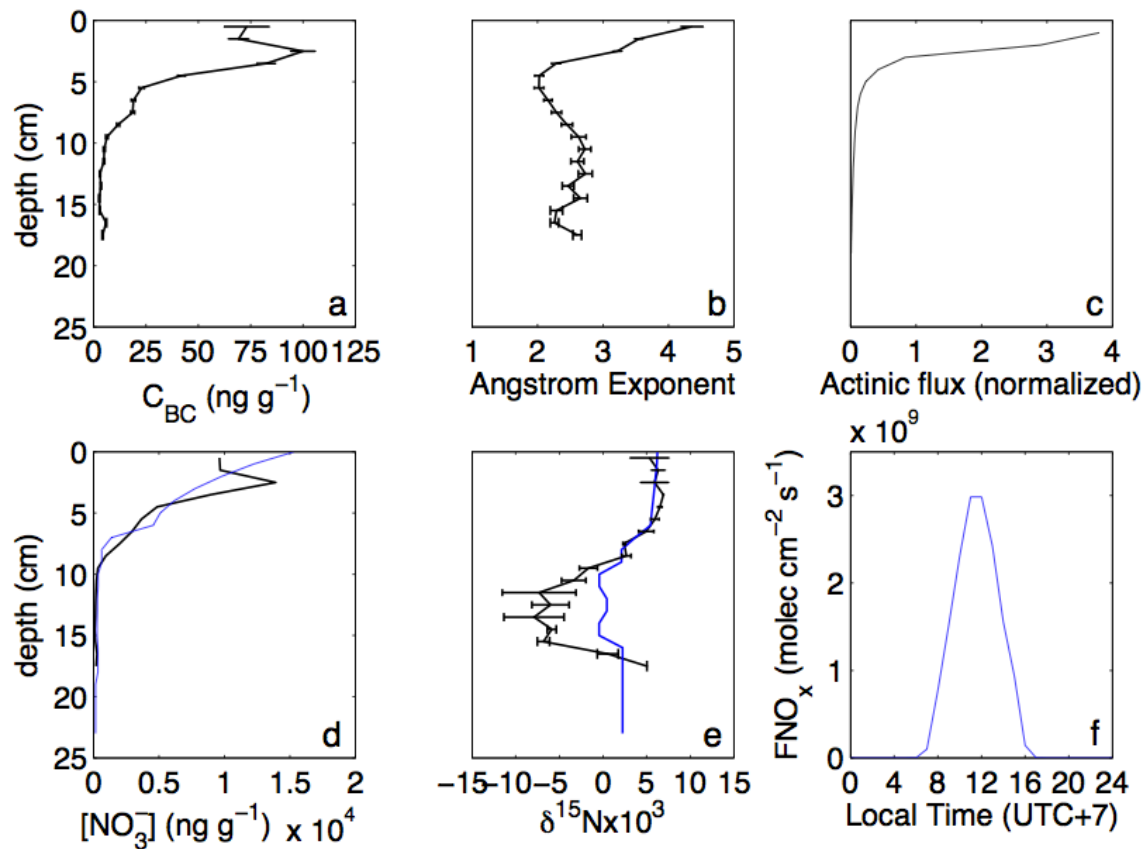


Figure 7A. Measured and modeled snow optical and chemical properties on January 22, 2014. Vertical profiles of (a) Measured black carbon concentrations ( $C_{BC}$ ,  $\text{ng g}^{-1}$ ), (b) Measured Ångström exponent for  $\lambda=450\text{-}600$  nm (unitless), (c) UV actinic flux normalized to surface downwelling irradiance, (d) Measured (black) and modeled (blue) nitrate concentrations ( $\text{ng g}^{-1}$ ), (e) Measured (black) and modeled (blue)  $\delta^{15}\text{N}(\text{NO}_3^-)$  when  $\Phi=4.6 \times 10^{-3}$  (‰), (f) Diurnal profiles of modeled snow-sourced  $F_{Nr}$  ( $\text{molec cm}^{-2} \text{s}^{-1}$ ) from TRANSITS.

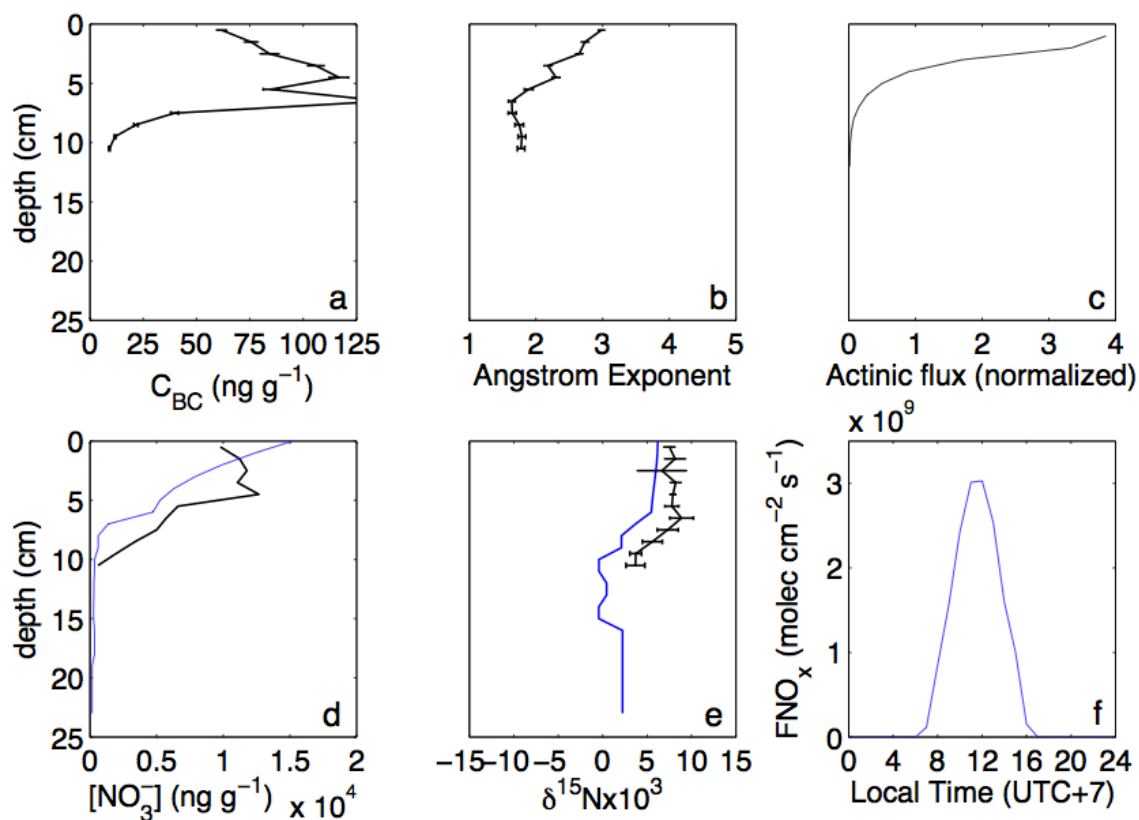


Figure 8A. Measured and modeled snow optical and chemical properties on January 24, 2014. Vertical profiles of (a) Measured black carbon concentrations ( $C_{BC}$ ,  $\text{ng g}^{-1}$ ), (b) Measured Ångström exponent for  $\lambda=450\text{-}600$  nm (unitless), (c) UV actinic flux normalized to surface downwelling irradiance, (d) Measured (black) and modeled (blue) nitrate concentrations ( $\text{ng g}^{-1}$ ), (e) Measured (black) and modeled (blue)  $\delta^{15}\text{N}(\text{NO}_3^-)$  when  $\Phi=4.6 \times 10^{-3}$  (‰), (f) Diurnal profiles of modeled snow-sourced  $F_{Nr}$  ( $\text{molec cm}^{-2} \text{s}^{-1}$ ) from TRANSITS.

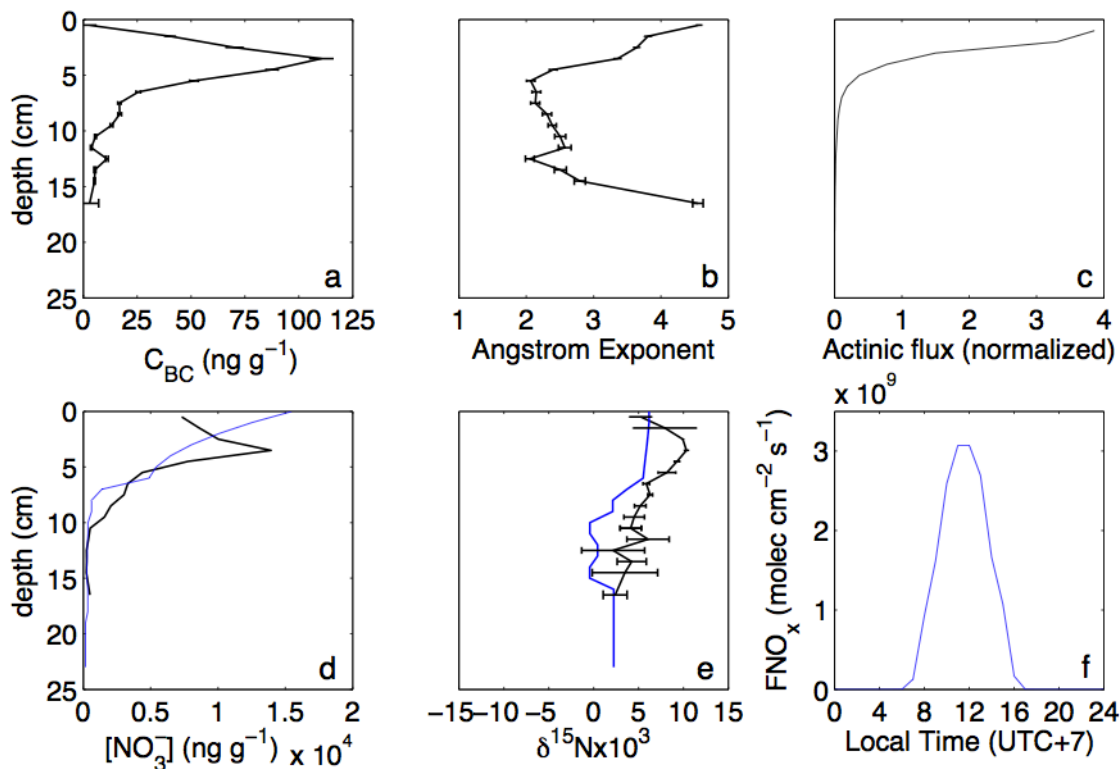


Figure 9A. Measured and modeled snow optical and chemical properties on January 26, 2014. Vertical profiles of (a) Measured black carbon concentrations ( $C_{BC}$ , ng g<sup>-1</sup>), (b) Measured Ångström exponent for  $\lambda=450-600$  nm (unitless), (c) UV actinic flux normalized to surface downwelling irradiance, (d) Measured (black) and modeled (blue) nitrate concentrations (ng g<sup>-1</sup>), (e) Measured (black) and modeled (blue)  $\delta^{15}N(NO_3^-)$  when  $\Phi=4.6 \times 10^{-3}$  (‰), (f) Diurnal profiles of modeled snow-sourced  $F_{NO_x}$  (molec cm<sup>-2</sup> s<sup>-1</sup>) from TRANSITS.

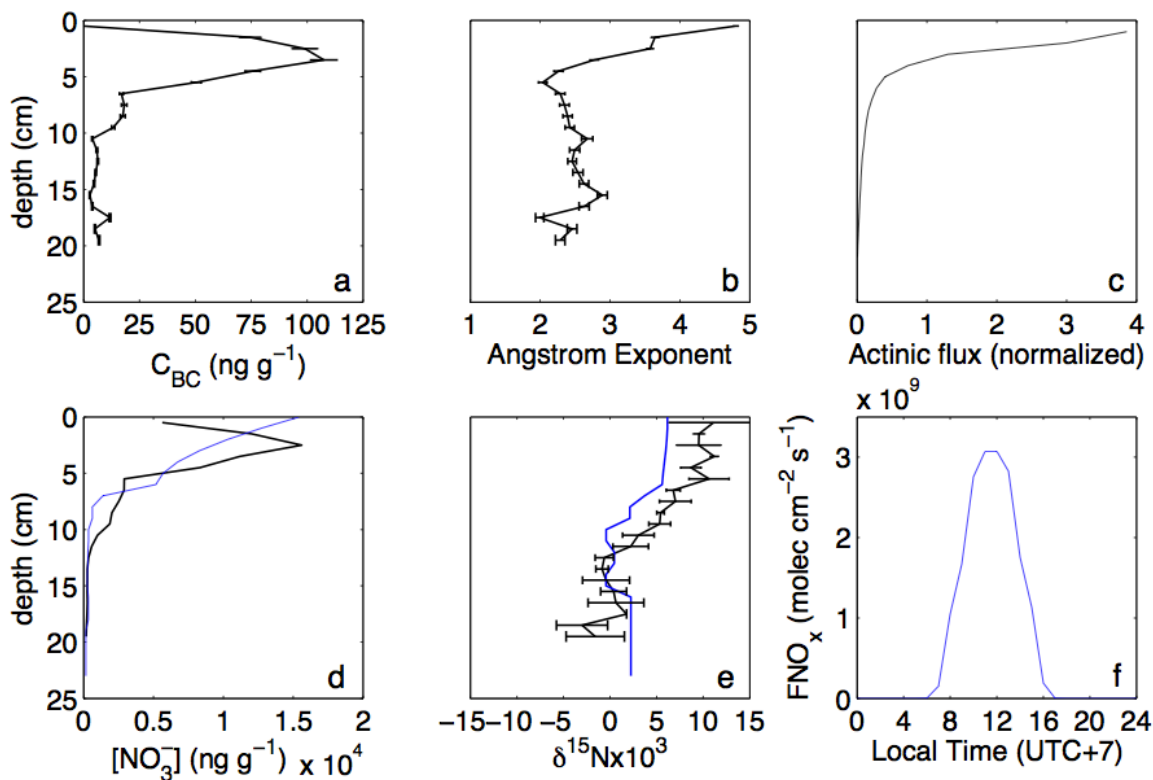


Figure 10A. Measured and modeled snow optical and chemical properties on January 29, 2014. Vertical profiles of (a) Measured black carbon concentrations ( $C_{BC}$ ,  $\text{ng g}^{-1}$ ), (b) Measured Ångström exponent for  $\lambda=450-600$  nm (unitless), (c) UV actinic flux normalized to surface downwelling irradiance, (d) Measured (black) and modeled (blue) nitrate concentrations ( $\text{ng g}^{-1}$ ), (e) Measured (black) and modeled (blue)  $\delta^{15}\text{N}(\text{NO}_3^-)$  when  $\Phi=4.6 \times 10^{-3}$  (‰), (f) Diurnal profiles of modeled snow-sourced  $F_{\text{NO}_x}$  ( $\text{molec cm}^{-2} \text{s}^{-1}$ ) from TRANSITS.

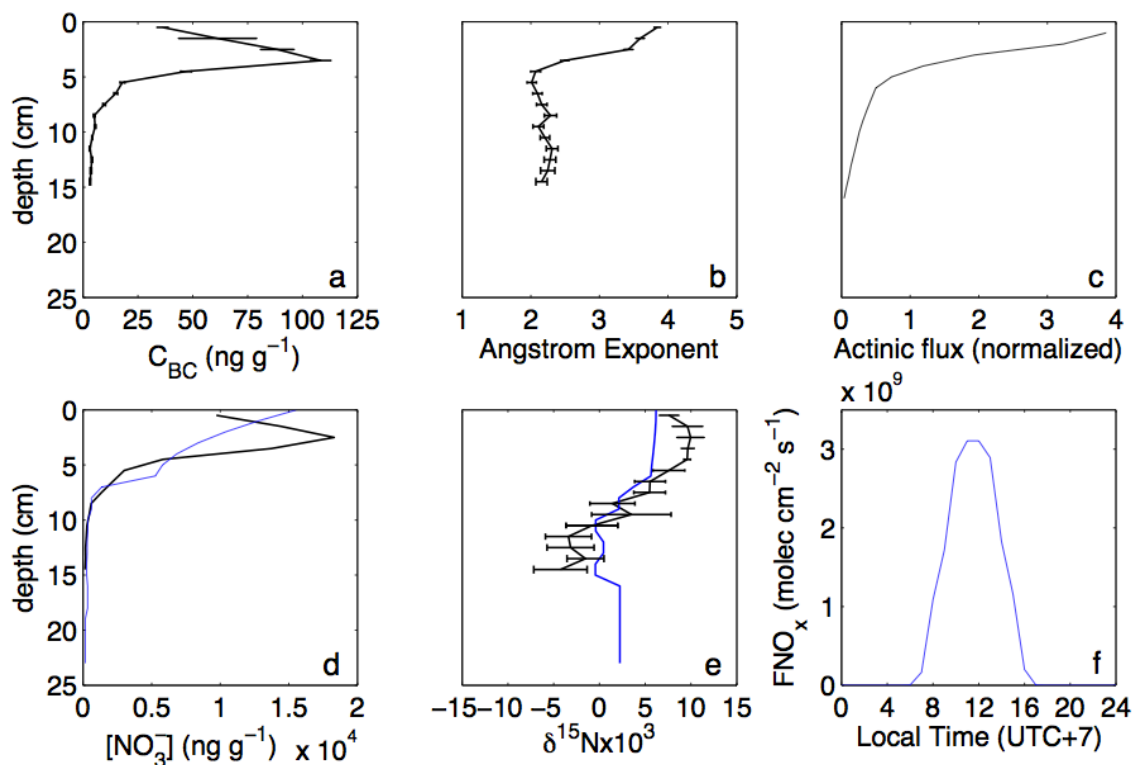


Figure 11A. Measured and modeled snow optical and chemical properties on January 30, 2014. Vertical profiles of (a) Measured black carbon concentrations ( $C_{BC}$ , ng g<sup>-1</sup>), (b) Measured Ångström exponent for  $\lambda=450-600$  nm (unitless), (c) UV actinic flux normalized to surface downwelling irradiance, (d) Measured (black) and modeled (blue) nitrate concentrations (ng g<sup>-1</sup>), (e) Measured (black) and modeled (blue)  $\delta^{15}N(NO_3^-)$  when  $\Phi=4.6 \times 10^{-3}$  (‰), (f) Diurnal profiles of modeled snow-sourced  $F_{Nr}$  (molec cm<sup>-2</sup> s<sup>-1</sup>) from TRANSITS.

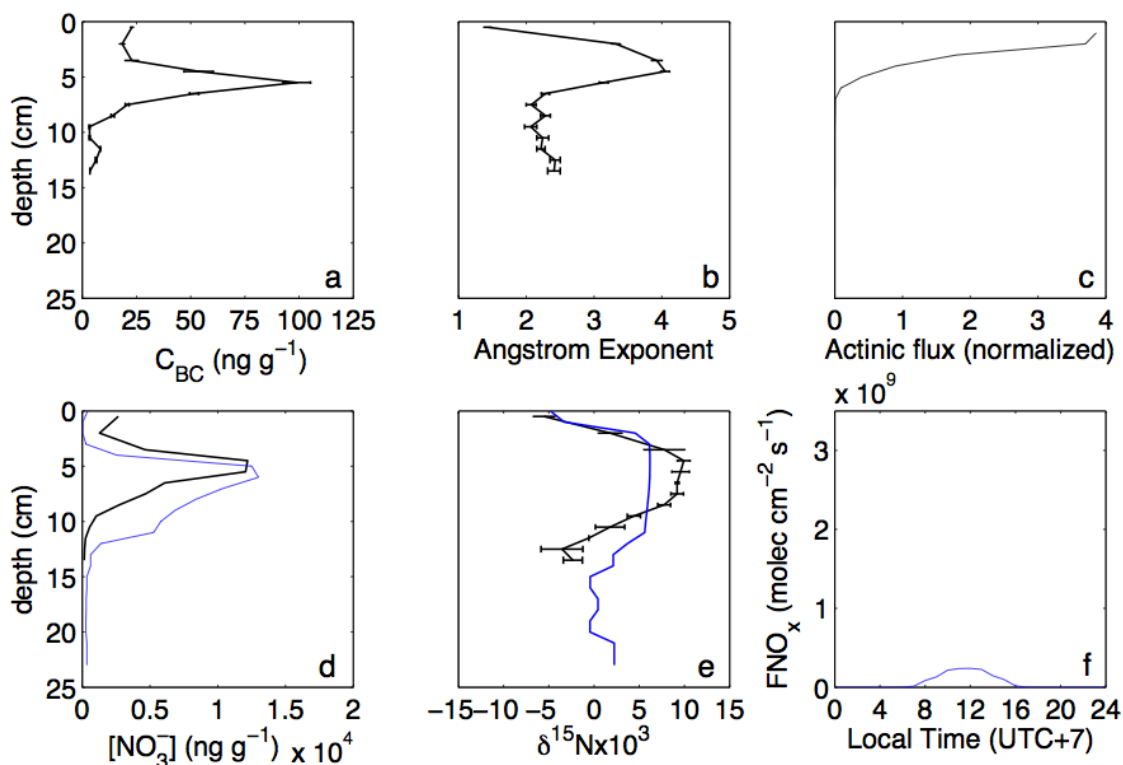


Figure 12A. Measured and modeled snow optical and chemical properties on January 31, 2014. Vertical profiles of (a) Measured black carbon concentrations ( $C_{BC}$ , ng g<sup>-1</sup>), (b) Measured Ångström exponent for  $\lambda=450-600$  nm (unitless), (c) UV actinic flux normalized to surface downwelling irradiance, (d) Measured (black) and modeled (blue) nitrate concentrations (ng g<sup>-1</sup>), (e) Measured (black) and modeled (blue)  $\delta^{15}N(NO_3^-)$  when  $\Phi=4.6 \times 10^{-3}$  (‰), (f) Diurnal profiles of modeled snow-sourced  $F_{NO_x}$  (molec cm<sup>-2</sup> s<sup>-1</sup>) from TRANSITS.

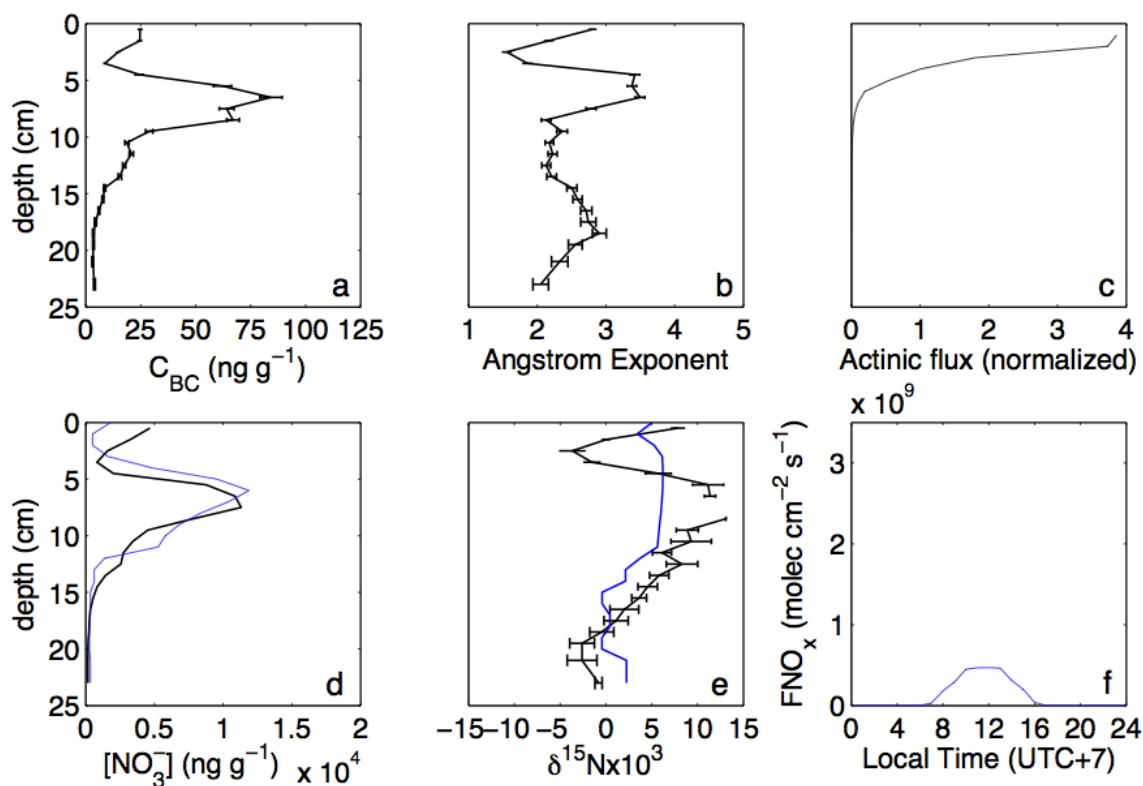


Figure 13A. Measured and modeled snow optical and chemical properties on February 4, 2014. Vertical profiles of (a) Measured black carbon concentrations ( $C_{BC}$ ,  $\text{ng g}^{-1}$ ), (b) Measured Ångström exponent for  $\lambda=450\text{-}600$  nm (unitless), (c) UV actinic flux normalized to surface downwelling irradiance, (d) Measured (black) and modeled (blue) nitrate concentrations ( $\text{ng g}^{-1}$ ), (e) Measured (black) and modeled (blue)  $\delta^{15}\text{N}(\text{NO}_3^-)$  when  $\Phi=4.6 \times 10^{-3}$  (‰), (f) Diurnal profiles of modeled snow-sourced  $F_{Nr}$  ( $\text{molec cm}^{-2} \text{s}^{-1}$ ) from TRANSITS.



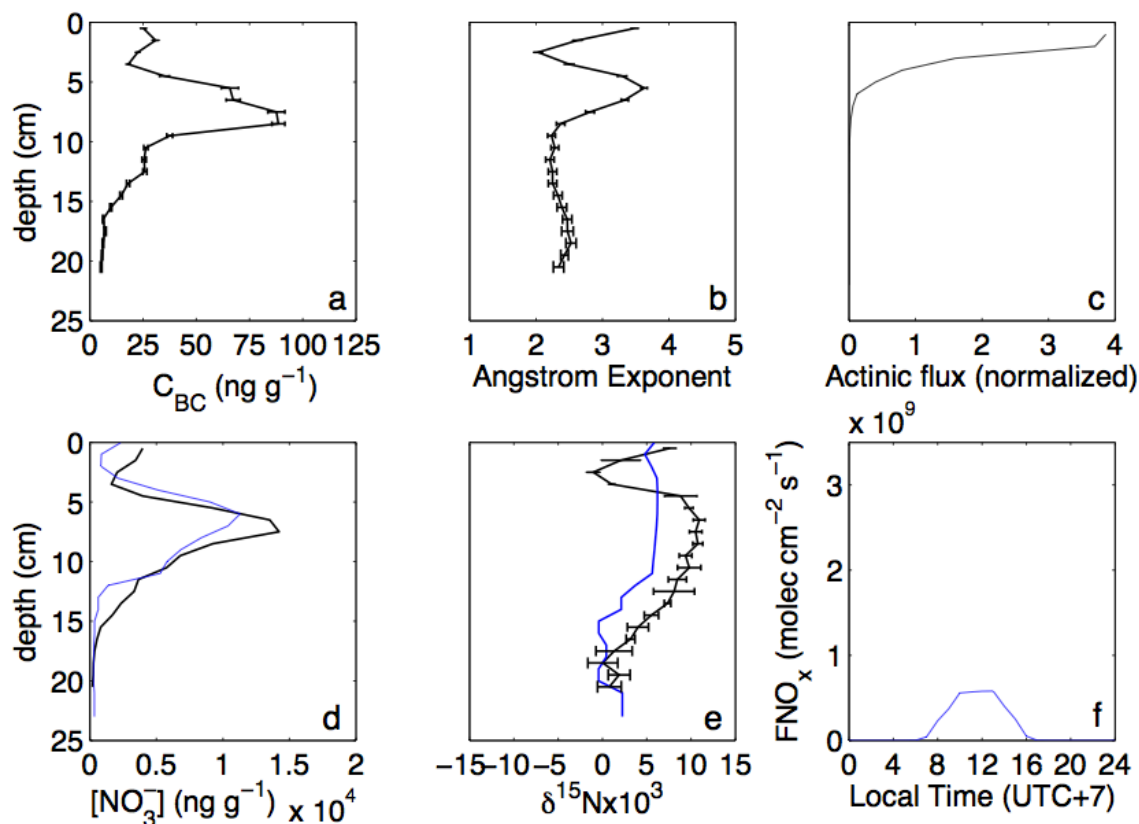


Figure 14A. Measured and modeled snow optical and chemical properties on February 6, 2014. Vertical profiles of (a) Measured black carbon concentrations ( $C_{BC}$ ,  $\text{ng g}^{-1}$ ), (b) Measured Ångström exponent for  $\lambda=450-600$  nm (unitless), (c) UV actinic flux normalized to surface downwelling irradiance, (d) Measured (black) and modeled (blue) nitrate concentrations ( $\text{ng g}^{-1}$ ), (e) Measured (black) and modeled (blue)  $\delta^{15}\text{N}(\text{NO}_3^-)$  when  $\Phi=4.6 \times 10^{-3}$  (‰), (f) Diurnal profiles of modeled snow-sourced  $F_{Nr}$  ( $\text{molec cm}^{-2} \text{s}^{-1}$ ) from TRANSITS.

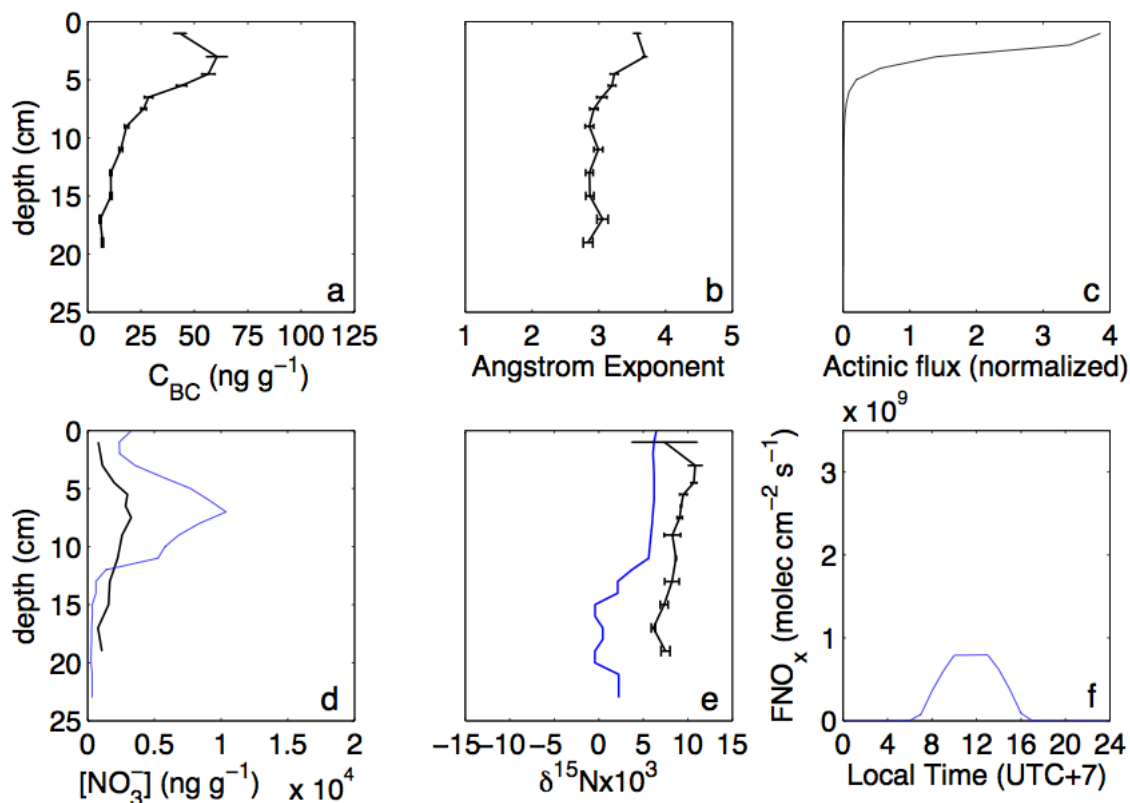


Figure 15A. Measured and modeled snow optical and chemical properties on February 11, 2014. Vertical profiles of (a) Measured black carbon concentrations ( $C_{BC}$ , ng g<sup>-1</sup>), (b) Measured Ångström exponent for  $\lambda=450-600$  nm (unitless), (c) UV actinic flux normalized to surface downwelling irradiance, (d) Measured (black) and modeled (blue) nitrate concentrations (ng g<sup>-1</sup>), (e) Measured (black) and modeled (blue)  $\delta^{15}N(NO_3^-)$  when  $\Phi=4.6 \times 10^{-3}$  (‰), (f) Diurnal profiles of modeled snow-sourced  $F_{Nr}$  (molec cm<sup>-2</sup> s<sup>-1</sup>) from TRANSITS.

# Supplemental Material B: Atmospheric observations and calculations

Table 1B. Modeled gas-phase ( $\text{HNO}_3$ ) and aerosol ( $\text{NO}_3^-$ ) nitrate dry-deposition flux to snow from model start date (12/19) to date of each snowpit<sup>a</sup>.

Pit	Deposition to snow ( $\text{kg nitrate m}^{-2} \text{ yr}^{-1}$ )		
	$\text{HNO}_3$	$\text{NO}_3^-$	$\text{HNO}_3 + \text{NO}_3^-$
1	$4.2 \times 10^{-6}$	$4.2 \times 10^{-6}$	$8.4 \times 10^{-6}$
2	$4.5 \times 10^{-6}$	$4.5 \times 10^{-6}$	$9.0 \times 10^{-6}$
3	$4.9 \times 10^{-6}$	$4.9 \times 10^{-6}$	$9.8 \times 10^{-6}$
4	$5.2 \times 10^{-6}$	$5.2 \times 10^{-6}$	$1.0 \times 10^{-5}$
5	$5.5 \times 10^{-6}$	$5.5 \times 10^{-6}$	$1.1 \times 10^{-5}$
6	$5.8 \times 10^{-6}$	$5.8 \times 10^{-6}$	$1.2 \times 10^{-5}$
7	$6.3 \times 10^{-6}$	$6.3 \times 10^{-6}$	$1.3 \times 10^{-5}$
8	$6.4 \times 10^{-6}$	$6.4 \times 10^{-6}$	$1.3 \times 10^{-5}$
9	$6.6 \times 10^{-6}$	$6.6 \times 10^{-6}$	$1.3 \times 10^{-5}$
10	$7.2 \times 10^{-6}$	$7.2 \times 10^{-6}$	$1.4 \times 10^{-5}$
11	$7.5 \times 10^{-6}$	$7.5 \times 10^{-6}$	$1.5 \times 10^{-5}$
12	$8.2 \times 10^{-6}$	$8.2 \times 10^{-6}$	$1.6 \times 10^{-5}$

<sup>a</sup>Dry-deposition of  $\text{HNO}_3$  and  $\text{NO}_3^-$  to snow is calculated using the campaign-averaged observed boundary layer mixing ratios for  $\text{HNO}_3$  ( $5784 \text{ ng m}^{-3}$ ) and  $\text{NO}_3^-$  ( $5777 \text{ ng m}^{-3}$ ) and an assumed dry-deposition velocity of  $0.03 \text{ cm s}^{-1}$ .

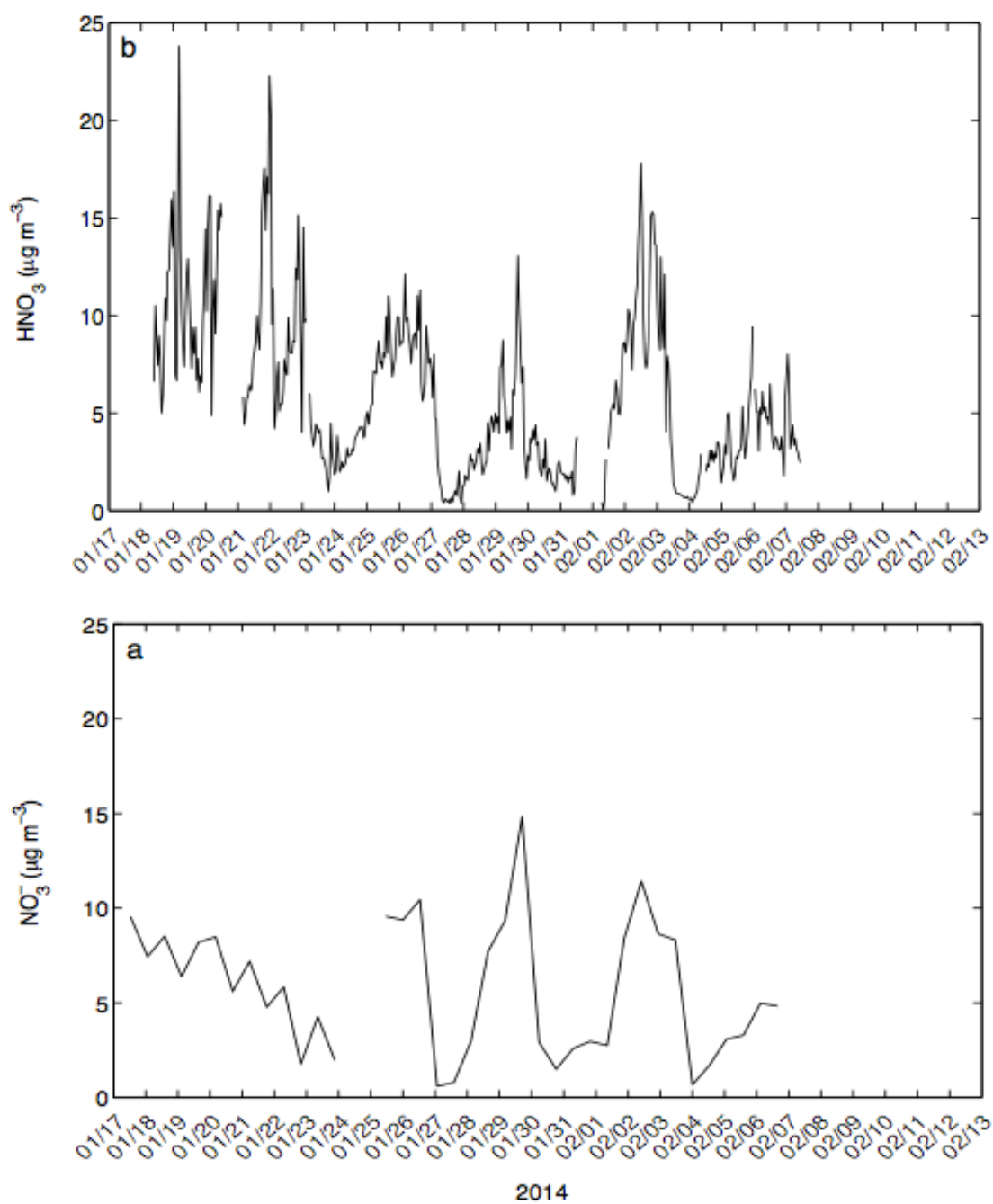


Figure 1B. (a) Atmospheric  $\text{NO}_3^-$  and (b)  $\text{HNO}_3$  during UBWOS2014 (units:  $\mu\text{g m}^{-3}$ ).  $\text{HNO}_3$  was measured every minute throughout the campaign and 1-hour averages are presented here.

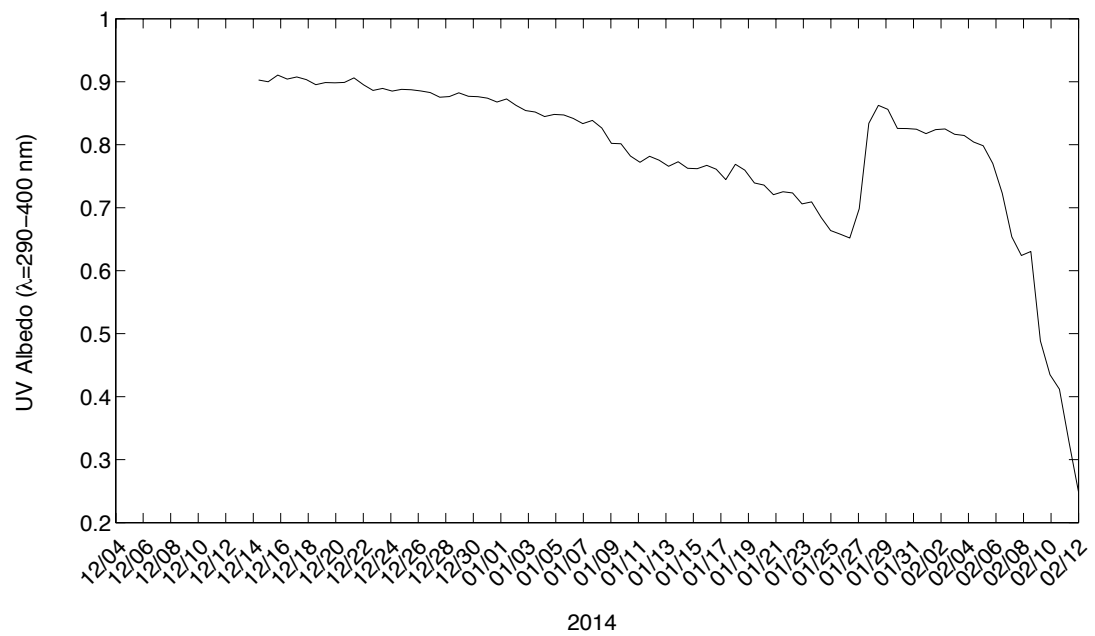


Figure 2B. Surface snow UV albedo ( $\lambda=290-400$  nm) measurements before and during the campaign.